Biomethane-derived Hydrogen for Proton Exchange Membrane Fuel Cells (PEMFCs): A Technical and Environmental Analysis through the Aspen Plus® Software

Benedicta Croce[a], Francesca Mennilli[a], Gabriele Comodi[a], and Mosè Rossi[a]

[a] Department of Industrial Engineering and Mathematical Science (DIISM), Marche Polytechnic University, Via Brecce Bianche 12, 60131 Ancona, Italy, b.croce@pm.univpm.it, CA, f.mennilli@pm.univpm.it, g.comodi@staff.univpm.it, mose.rossi@staff.univpm.it

Abstract:

The increasing demand for low-carbon energy systems has strengthened the role of hydrogen as a key energy carrier. While conventional hydrogen production mainly relies on fossil methane reforming, biomethane represents a renewable alternative with lower lifecycle emissions. In particular, when coupled with Proton Exchange Membrane Fuel Cells (PEMFCs), hydrogen derived from biomethane can enable efficient and flexible distributed power generation.

Despite the widespread use of process simulators in energy system design, the scientific literature still lacks robust modelling frameworks able to integrate biomethane reforming, gas purification, and electrochemical conversion within a single simulation environment.

This work develops an integrated Aspen Plus® model combining biomethane reforming, purification, and PEMFC conversion.

The model is based on real plant operating conditions, assuming a biomethane availability of about 150 Nm^3/h from an existing anaerobic digestion facility. A dedicated electrochemical sub-model, validated with experimental polarisation curves from the scientific literature, is implemented to reproduce fuel cell behaviour and realistic system-level energy balances.

Results show that the fuel processing section, comprising reforming, Water Gas Shift (WGS), and Selective Oxidation (SELOX), produces a hydrogen-rich stream of 211.7 m^3/h at 3 bar and 80°C, with methane conversion approximately 97% and Carbon Monoxide (CO) concentrations below 5 ppm, in strong agreement with scientific literature findings under similar operating conditions. The integrated system delivers a gross electrical output of approximately 360 kW and a recoverable thermal power of about 446.5 kW, corresponding to an overall Combined Heat and Power (CHP) efficiency of 85%. This thermal output fully meets the 400 kW heating demand of the anaerobic digesters while avoiding about 297 kg of Carbon Dioxide (CO_2)/h, equivalent to nearly 2,400 tCO_2 per year.

Keywords:

Biomethane; Energy Systems; Hydrogen; Numerical model; Proton Exchange Membrane Fuel Cell.

1. Introduction

Hydrogen is widely recognised as a key energy carrier for the decarbonisation of modern energy systems, particularly in sectors that are difficult to electrify, such as transportation, power generation, and energy-intensive industries. However, the environmental benefits of hydrogen are strongly dependent on the production pathway, as current global hydrogen supply still relies predominantly on fossil-based processes [1].

To address this challenge, the integration of hydrogen produced from biomethane with that generated via water electrolysis represents a more resilient decarbonisation strategy. While renewable hydrogen from electrolysis plays a central role in the energy transition, its large-scale deployment remains constrained by the intrinsic intermittency of primary Renewable Energy Sources (RESs) such as solar and wind power [2]. In this context, biomethane-based hydrogen production offers a complementary and dispatchable low-carbon

alternative. Compared to conventional natural gas reforming, biomethane reforming can significantly reduce lifecycle Carbon Dioxide (CO_2) emissions. According to Life Cycle Assessment (LCA) traditional fossil-based Steam Methane Reforming (SMR) generates between 10.09 and 17.21 $kgCO_2/kgH_2$, whereas utilising biomethane lowers the carbon footprint to a range of 1.20 to 8.60 $kgCO_2/kgH_2$ [3]. Furthermore, when combined with Carbon Capture and Storage (CCS) systems, this pathway may even achieve lower emissions, thereby contributing to net carbon removal while ensuring a stable and programmable energy supply [4].

Once produced, hydrogen can be efficiently converted into useful energy carriers. Among the available conversion technologies, Proton Exchange Membrane Fuel Cells (PEMFCs) stand out as a promising solution for decarbonising distributed power generation. Their high energy density, modular architecture, and fast dynamic response make them particularly well-suited for grid applications, where flexibility and dispatchability are essential. In such a context, the main challenge lies in the effective integration of renewable hydrogen production pathways, such as biomethane reforming, with downstream electrochemical conversion systems. Although Aspen Plus® has become a widely adopted tool for analysing complex energy systems, existing studies often focus on individual process stages rather than fully integrated biomethane-to-power configurations.

Amran et al. [5] developed a kinetic-based Aspen Plus® model for hydrogen production via SMR and subsequent Water Gas Shift (WGS), implementing Langmuir-Hinshelwood-Hougen-Watson (LHHW) reaction mechanisms within RPLUG reactors. The model was validated against experimental data, showing good agreement with a mean methane conversion error of approximately 3.3%. Sensitivity analysis indicated that hydrogen yield increases significantly between 500-700°C and with higher steam-to-methane ratios, while pressure effects were limited. Additionally, CO conversion in the WGS stage reached approximately 90% at a steam-to-CO ratio of 4.

Sinurat et al. [6] presented a simulation analysis of a PEMFC system using Aspen Plus®, focusing on the conversion of hydrogen chemical energy into electrical power and evaluating the stack performance at specific operating temperatures. The simulation revealed that a 135-cell stack generates 0.23 kW of power at a current density of $1 \cdot 10^{-3}$ A/m^2 and a Membrane Electrode Assembly (MEA) area of $3 \cdot 10^{-2}$ m^2, achieving a Nernst voltage of approximately 1.172 V while utilising 80% of the supplied hydrogen.

Barelli et al. [7] proposed a dynamic model for a 3 kW residential PEMFC acting as a Combined Heat and Power (CHP) unit. A preliminary 0D steady-state model was developed in Aspen Plus® to establish initial operating parameters, which were subsequently integrated into a comprehensive Matlab® Simulink dynamic simulation. The transient analysis indicated a rapid electrical power response of under 25 seconds and a thermal response ranging between 200 and 300 seconds. Furthermore, a sensitivity analysis demonstrated that maintaining the fuel cell at a 50% relative humidity yields the highest overall system efficiency.

Crespi et al. [8] developed a comprehensive Aspen Plus® model to optimise a flexible, MW-scale PEMFC power plant for grid balancing applications. The study demonstrated that system pressurization up to 1.7 bar significantly improves gross stack efficiency.

As highlighted by the reviewed studies, existing contributions tend to focus either on upstream hydrogen production processes or on downstream electrochemical conversion, often treating these aspects separately. As a result, fully integrated modelling approaches remain comparatively less explored in the scientific literature.

The novelty of the present work lies in the development of a comprehensive Aspen Plus® model that integrates the entire pathway from biomethane reforming to electrical and thermal power generation within a single simulation environment. In particular, the proposed approach couples the thermochemical section with a PEMFC model, whose performance is validated against scientific literature data, thereby ensuring the reliability of the electrochemical conversion stage.

Unlike studies primarily focused on detailed kinetic descriptions of individual reactors, this work adopts a thermodynamic equilibrium-based approach aimed at evaluating system-level interactions and overall energy performance. This integrated and validated framework enables a robust assessment of the biomethane-to-power conversion efficiency, while also providing a practical tool for preliminary design and techno-economic analysis of biomethane-derived hydrogen energy systems.

The paper is structured as follows: Section 2 describes the development and architecture of the simulation model, Section 3 presents the model integration within a real case study, Section 4 discusses the results obtained, and Section 5 reports the conclusions of the work.

2. Materials & methods

This section details the development and architecture of the simulation model. Specifically, Subsection 2.1 describes the standalone PEMFC model, whereas in Subsection 2.2 the fuel cell is coupled with a comprehensive reforming and purification line, incorporating the primary fuel conversion stage followed by WGS and Selective Oxidation (SELOX) units.

Figure 1 illustrates the plant layout, where the biomethane input is iteratively partitioned between the burner and the SMR. This logic-based split is calibrated to satisfy the reactor's thermal requirement (>750°C), assuming a 90% burner efficiency.

The process follows the following closed-loop logic: if the thermal threshold is not met, the split ratio will be systematically adjusted until computational convergence is achieved. After the thermal stabilisation, the syngas undergoes purification through WGS and SELOX stages before final electrochemical conversion in the fuel cell.

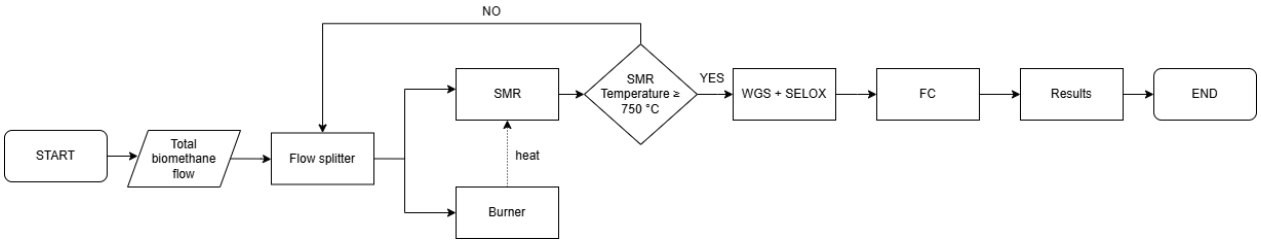

Figure 1. *Process flow diagram of the integrated SMR-FC system.*

2.1 PEMFC model development and validation

Regarding the PEMFC implementation in the Aspen Plus® environment, the NRTL-RK fluid package is selected for the modelling process. The operating conditions are set to 3 bar and 80°C to replicate the experimental setup from the literature upon which the model is validated. Under these conditions, the Non-Random Two-Liquid (NRTL) model accurately describes the non-ideal behaviour of liquid water, and the Redlich-Kwong (RK) equation of state accounts for gas phase deviations at moderate pressures. This combination is essential for a precise water balance and dew point calculation within the stack [9].

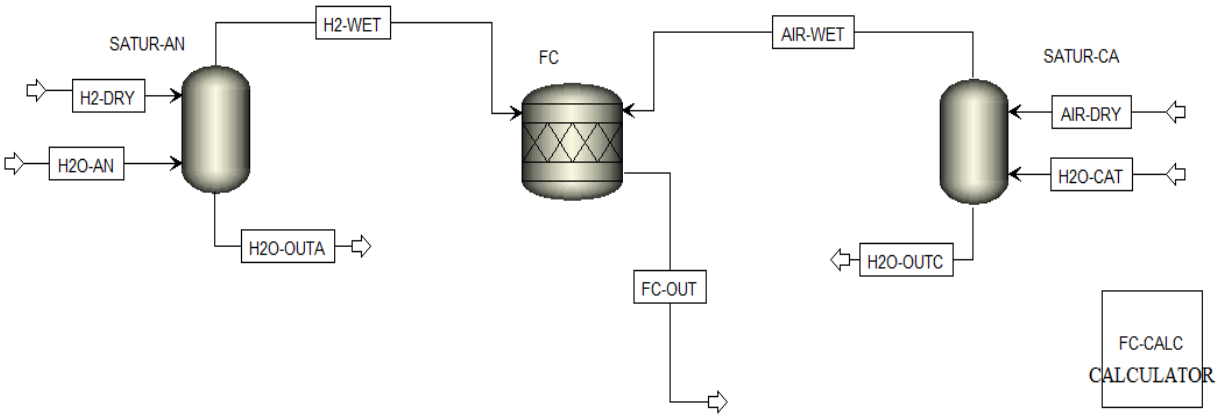

Figure 2. *PEMFC flowsheet.*

The flowsheet of the standalone fuel cell model, which is shown in Fig. 2, is designed to decouple the physical humidification process from the electrochemical reaction, thereby ensuring precise control of the inlet conditions. In particular, the humidification of both the anode and cathode streams is achieved through two flash separators, namely SATUR-AN and SATUR-CA, which act as gas saturators. These units mix the dry reactant streams (H2-DRY and AIR-DRY) with liquid water to generate humidified feeds (H2-WET and AIR-WET). This configuration enables accurate regulation of the inlet Relative Humidity (RH) before the electrochemical conversion within the stack. The PEMFC stoichiometric reactor (FC) represents the core unit of the model, where the global electrochemical reaction (R1) takes place. The reactor operates with a fuel utilisation factor (Uf) of 0.85 [7], allowing for a realistic representation of stack performance by accounting for the fraction of unreacted hydrogen in the anodic exhaust stream. The block evaluates the overall enthalpy change associated with the electrochemical reaction, corresponding to the maximum chemical energy available. This energy is subsequently partitioned into electrical power generation, determined through the electrochemical sub-model, while the remaining fraction contributes to the thermal output of the system.

$$H_2 + \frac{1}{2}O_2 \rightarrow H_2O, \ \Delta H^0_{298} = -285.8 \text{ kJ/mol.} \qquad \text{(R1)}$$

Since Aspen Plus® does not have a built-in library for fuel cell polarisation curves, a dedicated Calculator Block (FC-CALC) is also implemented. Indeed, the core of the model is governed by a set of electrochemical equations that relate the chemical potential of the reactants into electrical voltage.

The cell voltage (V) is calculated by subtracting the main voltage losses from the theoretical Nernst potential:

$$V_{cell} = E_{Nernst} - V_{act,c} - V_{act,\,a} - V_{Ohm} - V_{conc}. \qquad (1)$$

where E_{Nernst} is the Nernst' voltage (V), $V_{act,\,c}$ (V), and $V_{act,\,a}$ (V) are the activation overpotential of cathode and anode, respectively, V_{Ohm} (V) is the ohmic overpotential, and V_{conc} (V) is the mass transport overpotential.

The Nernst potential represents the reversible open-circuit voltage and is calculated based on the operating temperature and the partial pressures of reactants and products:

$$E_{Nernst} = E_0(T) + \frac{R \cdot T}{n \cdot F} \ln\left(\frac{P_{H2} \cdot P_{02}^{0.5}}{P_{H2O}}\right). \qquad (2)$$

In particular, $E_0(T)$ is the standard potential at temperature T *(K);* R (J/(mol·K)) is the gas constant, F (C/mol) is the Faraday constant, n is the number of electron exchanged, and p_{H2}, p_{O2}, p_{H2O} are the partial pressures of the reactants hydrogen and Oxygen (O_2) and of the product water, respectively.
The temperature-dependent standard potential $E_0(T)$ is calculated using an empirical correlation:

$$E_0(T) = 1.299 - 0.9 \cdot 10^{-3} \cdot (T - 298). \qquad (3)$$

The activation losses are associated with the chemical energy barrier that must be overcome to start the electrochemical reactions at the electrode's surface.

In a PEMFC, the kinetics of the two electrodes are highly asymmetric; indeed, while the Hydrogen Evolution Reaction (HER) at the anode is extremely fast and occurs with minimal resistance, the Oxygen Evolution Reaction (OER) at the cathode is significantly slower and represents the primary source of voltage loss. For this reason, the anodic activation overpotential is often considered negligible in comparison to the cathodic one [10]. Eqs. (4) and (5) report the activation overpotential for both the cathode and anode electrodes, calculated using the Tafel's expression, where α_c and α_a are the dimensionless charge transfer coefficients, i is the operating current density (A/cm^2), and $i_{0,c}$ and $i_{0,a}$ represent the exchange current densities (A/cm^2) for the cathode and anode, respectively:

$$V_{act,c} = \frac{R \cdot T}{\alpha_C \cdot n \cdot F} \cdot \ln\left(\frac{i}{i_{o,c}}\right), \qquad (4)$$

$$V_{act,a} = \frac{R \cdot T}{\alpha_a \cdot n \cdot F} \cdot \ln\left(\frac{i}{i_{o,a}}\right). \qquad (5)$$

The ohmic overpotential follows the Ohm's law and accounts for the resistive losses associated with proton transport through the polymer membrane and electron conduction across the cell's conductive components, including the bipolar plates and gas diffusion layers.

The total cell resistance R_{cell} is dominated by the ionic resistance of the polymer membrane [11], which is defined as the ratio between electrolyte thickness δ and its ionic conductivity σ.

$$V_{Ohm} = R_{cell} \cdot i = \frac{\delta}{\sigma} \cdot i. \qquad (6)$$

The mass transport overpotential represents the voltage loss arising when the rate of reactant consumption at the electrode surface exceeds the rate at which species can be supplied from the bulk gas phase. This limitation becomes particularly significant at high current densities where concentration gradients develop and lead to a pronounced decline in cell voltage. The theoretical expression describing this loss is given by:

$$V_{conc} = -\frac{R \cdot T}{n \cdot F} \cdot \ln\left(1 - \frac{i}{i_L}\right). \quad (7)$$

where i_L (A/cm^2) represents the limiting current density.

In this study, the fuel cell is simulated within the ohmic region; therefore, mass transport phenomena can be neglected.

The electrochemical model presented above incorporates several parameters that are intrinsically dependent on the specific cell architecture and material properties that, in this case, have been taken from the scientific literature [12]. To ensure an accurate representation of the PEMFC performance under well-defined operating conditions, namely a temperature of 80°C, a relative humidity of 100%, and an operating pressure of 3 bar, an optimisation procedure was carried out in the Python programming environment to determine the main kinetic coefficients of the system. The geometric parameters and baseline operating quantities adopted from the scientific literature are reported in Table 1.

Table 1. *Geometric parameters [12].*

Parameter	Symbol	Value	U.M.
Active area	A_{act}	51.84	cm^2
Membrane thickness	δ	127	μm
Anodic/cathodic Pt loading	L_{Pt}	0.4	mg$_{Pt}$/cm^2

These values define the physical configuration of the cell and serve as fixed inputs to the model. Conversely, the key electrochemical parameters, namely the cathodic exchange current density ($i_{0,c}$), the cathodic charge transfer coefficient (α_c), and the membrane ionic conductivity (σ), were estimated through a curve-fitting procedure and are summarised in Table 2.

The fitting procedure was implemented in an open-source Python environment by minimising the deviation between the simulated voltage response and the corresponding experimental polarisation data obtained from the scientific literature [12]. The resulting set of fitted parameters defines the calibrated state of the model and is subsequently implemented within the FC-CALC Calculator Block, ensuring that the simulated voltage response accurately reproduces that of the reference system.

Based on the polarisation curve used to derive the electrochemical formulation implemented in the Aspen Plus® model, a maximum operating point was identified within the ohmic region at a current density of 1.25 A·cm^{-2}, and cell voltage of 0.56 V under the specified operating conditions [12]. By considering the active area of the laboratory-scale reference cell, the resulting cell current is equal to 64.8 A.

To estimate the thermal power generated by the fuel cell, the net duty of the FC-CALC block in Aspen Plus® is used. Since the software does not include a built-in fuel cell model, it does not directly separate the total energy into electrical and thermal components. Therefore, the thermal power is obtained by subtracting the electrical contribution from the total energy provided by Aspen Plus®, effectively isolating the heat generated within the system.

To validate this estimation, the maximum thermal power is alternatively calculated using the electrochemical relation:

$$Q = I \cdot (E_{tn} - V_{cell}). \quad (8)$$

where I (A) is the cell current, E_{tn} (V) is the theoretical thermoneutral potential, and V_{cell} is the measured cell voltage. This approach accounts for electrical losses and provides a direct comparison with the heat obtained from the Aspen Plus® net duty approach.

Table 2. *Fitted electrochemical parameters.*

Parameter	Symbol	Value	U.M.
Cathodic charge transfer coefficient	α_c	0.5	-
Reference cathodic exchange current density	$i_{0ref,c}$	$9.8 \cdot 10^{-9}$	A/cm^2
Membrane ionic conductivity	σ	0.072	S/m

2.2. Hydrogen production and purification section

The proposed multi-stage process is designed to convert biomethane into a high-purity hydrogen stream suitable for fuel cell applications, with particular emphasis on heat integration to enhance overall system efficiency. As illustrated in Fig. 3, the incoming biomethane stream is divided into two fractions: a fuel stream (BIOM) directed to the burner, assumed to operate at a thermal efficiency of 90% [13], and a process feedstock stream (BIOM-1) supplied to the reforming section.

Feedstock preparation begins with the compression of BIOM-1 in COMPR-1, while the liquid water stream is pressurised and preheated in heat exchanger HX-1 by recovering sensible heat from the water-gas shift reactor outlet (WGS-OUT). After mixing the preheated water with the compressed biomethane, the desired steam-to-carbon (S/C) ratio is established. The resulting mixture is then fully vaporised and superheated in HX-2 using high-temperature heat recovered from the SMR effluent.

The conditioned feed subsequently enters the SMR reactor, where catalytic reforming produces a hydrogen-rich syngas. The hot reformate is cooled in HX-2 to support feed vaporisation and then directed to the WGS reactor to maximise hydrogen production through the exothermic shift reaction. Further cooling in HX-1 enables additional heat recovery and temperature conditioning prior to final CO removal in SELOX unit. This purification sequence reduces CO concentrations to ppm levels, ensuring the hydrogen stream meets the purity requirements for downstream PEMFC operation.

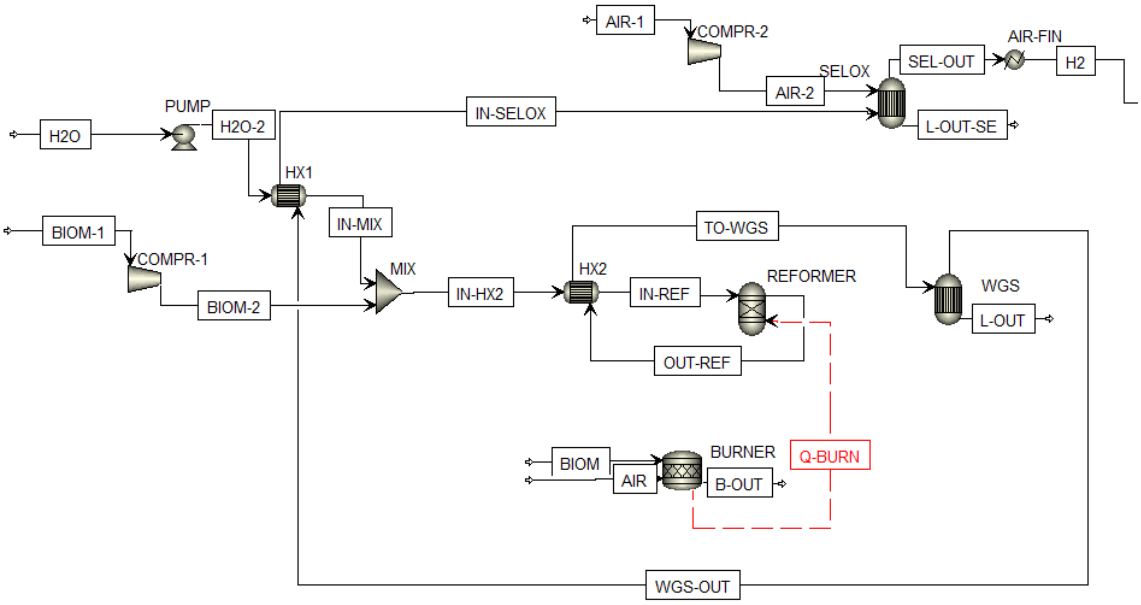

Figure 3. *Flowsheet of reforming process with burner heat integration.*

The conversion of biomethane into high-purity hydrogen is achieved through a sequence of reactors, each modelled using specific blocks to ensure thermodynamic consistency and industrial realism.

The reformer reactor is modelled using the RGIBBS block, which determines the product distribution by minimizing the total Gibbs free energy [14]. The reactions occurring simultaneously within the reformer are the SMR described in Reaction (R2) and the WGS described in Reaction (R3):

$$CH_4 + H_2O \leftrightarrow CO + 3H_2, \quad \Delta H^0_{298} = 206 \text{ kJ/mol}, \qquad \text{(R2)}$$

$$CO + H_2O \leftrightarrow CO_2 + H_2, \quad \Delta H^0_{298} = -41 \text{ kJ/mol}. \qquad \text{(R3)}$$

The purification stages are modelled using REQUIL blocks according to the validated model in [15]. In the WGS unit, Reaction (R2) is promoted at lower temperatures to favour the exothermic equilibrium; therefore, the reformer effluent is cooled through the HX-2 heat exchanger before entering the reactor to maximize the H_2 yield.

Final CO abatement is achieved via selective oxidation, as described in Reaction (R4), to reduce the CO content to ppm levels:

$$2CO+O2 \leftrightarrow 2CO_2,\ \Delta H^0_{298} = -283\ kJ/mol. \quad (R4)$$

To provide the thermal duty required for the endothermic SMR process, a fraction of the total biomethane feed is diverted to a burner, modelled using the RSTOIC block. The combustion reactions are described in Reactions (R5):

$$CH_4+2O_2 \rightarrow CO_2+2H_2O,\ H^0_{298} = -\ 802\ kJ/mol. \quad (R5)$$

3. Case Study

This section evaluates the proposed system through a case study based on an existing agricultural biogas plant. The reference facility operates thermophilic anaerobic digesters at 47-48°C, requiring a constant thermal input of 400 kW to ensure process stability. In addition, the plant provides a benchmark for the achievable biomethane production capacity.

However, it is worth noting that the biogas production and upgrading processes are not simulated, as they are outside the scope of the present work. Indeed, the system boundary is defined at the outlet of the upgrading unit, and a constant biomethane stream of 150 Nm^3/h is assumed as input to the model.

The biomethane stream is divided into two flows: (i) a process fuel stream (BIOM-1), which is fed to the SMR unit for hydrogen production, and (ii) an auxiliary fuel stream (BIOM), which is supplied to the burner. The burner is sized to provide the heat required for the endothermic reforming reactions, considering heat recovery from the system's heat exchangers. To account for the burner's 90% efficiency, the biomethane flow available for the auxiliary stream is reduced to approximately 143.5 Nm^3/h. Based on the Aspen Plus® results, the burner requires approximately 58.5 Nm^3/h of biomethane; when considering the burner efficiency, the actual fuel demand increases to roughly 65.0 Nm^3/h.

Table 3 details the thermophysical evolution of the process streams. Beyond the initial inlet conditions (25°C and 1 bar), the plant is pressurized to 3 bar to align the simulation with the PEMFC experimental benchmarks used for model validation.

This pressurized regime is maintained across the fuel cell electrodes, with the stack temperature fixed at 80°C to reflect typical low-temperature operation. To optimize hydrogen yield, a steam-to-carbon (S/C) ratio of 3 was implemented within the reforming section, effectively preventing carbon deposition [16].

Table 3. *Main characteristics of process streams in the Aspen Plus® simulation.*

Stream	Temperature (°C)	Pressure (atm)	Mass (kg/h)	Volume (m^3/h)	Stream	Temperature (°C)	Pressure (atm)	Mass (kg/h)	Volume (m^3/h)
BIOM	25.0	1.0	43.3	63.7	IN-REF	138.6	3.0	266.7	168.3
AIR	25.0	1.0	906.1	770.2	OUT-REF	773.8	3.0	266.7	640.9
B-OUT	800.0	1.0	949.5	3004.4	TO-WGS	148.6	3.0	266.7	257.7
BIOM-1	25.0	1.0	61.9	92.5	WGS-OUT	262.6	3.0	266.7	327.8
BIOM-2	137.4	3.0	61.9	42.5	IN-SELOX	135.1	3.0	266.7	249.6
H2O	25.0	1.0	204.8	0.21	AIR-1	25.0	1.0	24.3	20.6

Stream	Temperature (°C)	Pressure (atm)	Mass (kg/h)	Volume (m³/h)	Stream	Temperature (°C)	Pressure (atm)	Mass (kg/h)	Volume (m³/h)
H2O-2	25.0	3.0	204.8	0.21	AIR-2	176.2	3.0	24.3	10.3
IN-MIX	125.1	3.0	204.8	0.23	SEL-OUT	195.3	3.0	291.0	296.4
IN-HX2	88.7	3.0	266.7	47.1	H2	80.0	3.0	291.0	211.7
H2O-AN	25.0	3.0	100.0	0.10	H2-WET	80.0	3.0	276.1	215.2
H2O-CAT	25.0	3.0	100.0	0.10	H2O-OUTA	80.0	3.0	114.9	0.12
AIR-DRY	25.0	1.0	1178.3	998.6	AIR-DRY1	176.2	3.0	1178.3	502.3
AIR-WET	80.0	3.0	1278.3	447.2	FC-OUT	80.0	3.0	1554.4	474.5

4. Results and discussion

This section evaluates the performance of the developed model from chemical, energetic, and environmental perspectives. The analysis first examines hydrogen production, including flow rates, stream composition, and reforming efficiency. It then assesses system energy performance in terms of electrical and thermal outputs and overall efficiency. Finally, the environmental impact is evaluated by comparing biomethane-based operation with a fossil methane benchmark, highlighting the potential for decarbonisation.

4.1. Hydrogen production and stream composition

The hydrogen-rich stream produced by the reforming process has a volumetric flow rate of approximately $5.86 \cdot 10^{-2}$ m^3/s at 25°C and 3 bar, corresponding to a mass flow rate of about $8.08 \cdot 10^{-2}$ kg/s.

The stream is predominantly composed of hydrogen (61.8% mol), water vapor (19.0% mol), and CO_2 (16.0% mol), together accounting for nearly 97% of the total mixture. This high hydrogen content confirms the effectiveness of the reforming process, while the significant steam fraction ensures proper humidification of the membrane in the PEMFC, thus reducing the need for external water management.

The selectivity of the purification stages is demonstrated by the low residual methane content around 0.33% mol, corresponding to a methane conversion efficiency of approximately 97%. CO levels are maintained strictly below 5 ppm, effectively eliminating the risk of catalyst poisoning in the fuel cell anode.

Finally, the presence of Nitrogen (N_2) (2.8% mol) and a safe O_2 surplus (0.04% mol) is exclusively related to the air injection in the SELOX unit. This air supply is precisely calibrated to ensure the complete oxidation of CO into CO_2 before the gas enters the electrochemical section.

4.2. Energy analysis

The thermal balance of the reforming section is primarily governed by the heat duty provided by the external burner and the internal heat recovery network. The SMR reaction requires a net heat duty of 326.6 kW, which is supplied through an external burner. Considering a burner efficiency of 90%, the total heat released by combustion is approximately 363 kW. This high-grade heat is entirely dedicated to the chemical cracking of biomethane molecules within the reformer tubes.

To maximise the overall thermal efficiency of the system, the plant implements a two-stage heat recovery cascade designed to progressively increase the enthalpy of the reactants from their inlet conditions up to the reformer entrance by recovering sensible heat from the hot product streams. In the first stage (HX-1), the water feed directed to the reactant mixer is preheated from 25°C to 125.1°C by recovering heat from the hot syngas exiting the SELOX unit, resulting in a recovered thermal power of 26.0 kW. This step enhances the sensible heat content of the water before mixing with biomethane. In the second stage (HX-2), the partially heated process mixture is further increased in temperature from 88.7°C to 138.6°C prior to entering the catalytic reformer. This is achieved by exploiting the high-temperature enthalpy of the raw syngas leaving the reformer, which is simultaneously cooled from 773.8°C to 148.6°C, allowing the recovery of 130.7 kW. This stage is crucial both for adequately conditioning the feed for the endothermic reforming reactions and for reducing the temperature of the syngas to conditions more suitable for the downstream WGS process, where lower temperatures favour the exothermic equilibrium.

In addition to thermal integration, the SMR section requires electrical energy to drive process stream compression. The biomethane feed is compressed to the operating pressure of 3 bar in COMPR-1, with a power consumption of 4.5 kW, while COMPR-2 supplies air to the SELOX reactor for selective CO oxidation, requiring 1.0 kW.

4.2.1. PEMFC stack and net system balance

The total electrical power output of the system, provided by the fuel cell stack, is 360 kW. By subtracting this value from the total reaction enthalpy predicted by the Aspen Plus® model (approximately 860 kW), a residual thermal power of 500 kW is obtained.

The validation performed by applying Eq. (8) yields a thermal power of 590 kW, corresponding to a 18% deviation from the Aspen Plus® predictions. This discrepancy arises because Aspen Plus® does not inherently incorporate an electrochemical model within its energy balance framework and, therefore, neglects electrochemical irreversibility such as activation, ohmic (Joule heating), and concentration losses that physically manifest as additional heat generation in the real system.

In agreement with performance benchmarks reported in the literature, an overall CHP efficiency of 85% was adopted for the final energy balance. This results in a net recoverable thermal power of 446.5 kW (47% of the input energy), accounting for the typical 15% energy loss associated with exhaust streams and stack surface dissipation in industrial-scale PEMFC systems [17].

Table 4 presents the thermal energy distribution, including both the heat supplied to the SMR section and the recoverable heat from the fuel cell stack.

***Table 4**. Summary of thermal power flows in reforming and PEMFC systems.*

Section	Energy stream	Power (kW)
Reforming	External burner	326.6
Reforming	HX-1	26.0
Reforming	HX-2	130.7
PEMFC	Residual heat from Aspen calculation	500.0
PEMFC	Residual heat from Eq. (8)	590.0
PEMFC	Net recoverable heat from Aspen Plus®	425.0
PEMFC	Net recoverable heat from Eq. (8)	446.5

Consequently, the net recovered thermal power of 446.5 kW meets the nominal thermal demand of the anaerobic digesters. This substantial thermal surplus provides a critical operational safety margin, ensuring reliable compensation for thermal peaks during winter months when heat losses from the digester tanks increase significantly due to low ambient temperatures.

To determine the net electrical output of the integrated plant, the total internal self-consumption (parasitic loads) must be deducted from the gross stack production. The largest energy draw is the cathode air compressor (COMPR-3), which consumes 50.3 kW. In addition, the PEM stack is designed to supply the electrical demand of the SMR section, specifically the feed and process compressors (COMPR-1 and COMPR-2), which require 4.5 kW and 1.0 kW, respectively. The total internal electrical consumption amounts to 55.8 kW, representing approximately 15.5% of the gross electrical power generated by the stack. Therefore, the final net electrical power delivered by the system is 304.2 kW.

Table 5 reports the electrical energy flows, detailing the gross stack production, parasitic loads, and the resulting net electrical output available for the integrated plant.

***Table 5.** Electrical energy distribution in the reforming and PEMFC system.*

Section	Energy stream	Power (kW)
Reforming	COMPR-1	4.5
Reforming	COMPR-2	1.0
PEMFC	Gross stack output	360.0

Section	Energy stream	Power (kW)
PEMFC	COMPR-3	50.3
PEMFC	Total internal consumption	55.8
PEMFC	Net electrical output	304.2

Figure 4 illustrates the energy distribution across the two main subsystems of the plant: the reforming section and the PEMFC. For each section, the figure highlights the breakdown of useful energy, recovered heat, and losses, providing a quantitative overview of the internal energy flows.

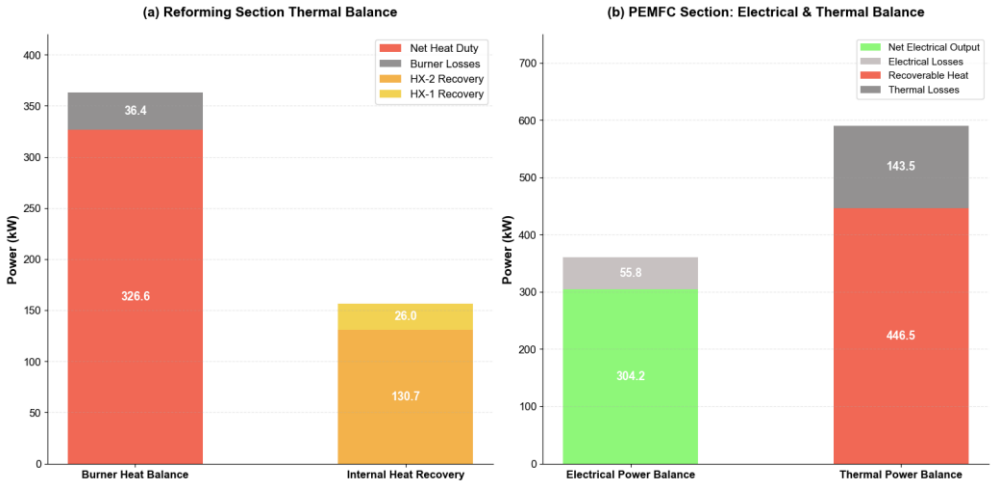

Figure 4. *Energy analysis of the integrated system: (a) Thermal power balance and heat recovery breakdown for the SMR section; (b) Electrical and thermal power distribution of the PEMFC system, including parasitic loads and environmental losses.*

4.3. Environmental analysis

The environmental benefit of the integrated system is quantified by evaluating the avoided CO_2 emissions resulting from the substitution of fossil natural gas with biomethane. This substitution occurs across two subsystems: the burner, 65 Nm^3/h), and the SMR process, 85 Nm^3/h.

From a carbon mass balance perspective, both combustion in the burner and feedstock conversion in the reformer lead to the complete oxidation of the inlet carbon. Specifically, the stoichiometric reactions for combustion (R5) and for SMR combined with the WGS (R2 and R3) indicate that one mole of methane produces exactly one mole of CO_2. Accordingly, following the IPCC Guidelines for National Greenhouse Gas Inventories, both stationary combustion and industrial hydrogen production adopt the same carbon-based default emission factor for natural gas, set at 56.1 kg CO_2/GJ [18].

However, since the CO_2 released by the integrated plant originates entirely from biomethane, it is considered biogenic carbon. Under the IPCC accounting framework, biogenic CO_2 emissions are reported solely for informational purposes and are not included in the national greenhouse gas inventory, effectively resulting in a net-zero climate impact.

Considering a total biomethane consumption of 150 Nm^3/h and assuming a standard lower heating value of 0.0353 GJ/Nm^3, the process substitutes approximately 5.295 GJ/h of fossil energy. Applying the IPCC default emission factor, the plant avoids direct emissions of 297.1 kg CO_2/h. Assuming 8,000 equivalent operating hours per year, this corresponds to a total greenhouse gas mitigation of approximately 2,376 tCO_2 per year, fully decarbonizing both hydrogen production and power generation pathways.

5. Conclusions

This study presents a comprehensive simulation framework developed in Aspen Plus® to model the integration of biomethane reforming, gas purification, and PEMFC power generation. By coupling rigorous thermodynamic process modelling with a validated electrochemical sub-model.

Application to a reference anaerobic digestion facility (with a biomethane capacity of 150 Nm^3/h) demonstrated the technical viability of the proposed architecture. The multi-stage processing sequence, comprising SMR, WGS, and SELOX unit, achieved a methane conversion efficiency around 97%. The system reliably generated a fuel-cell-grade hydrogen stream ($5.86 \cdot 10^{-2}$ m^3/s) while strictly maintaining CO concentrations below 5 ppm, thereby effectively mitigating the risk of anode catalyst poisoning.

The PEMFC stack yielded a gross electrical output of 360 kW, which translates to a net electrical power delivery of 304.2 kW after deducting internal parasitic loads (55.8 kW), primarily driven by reactant compression. Furthermore, the system recovered 446.5 kW of net thermal power. This thermal output entirely satisfies the 400 kW baseline heating demand of the thermophilic anaerobic digesters, while providing an essential operational margin to offset seasonal heat losses and ensure plant thermal self-sufficiency.

From an environmental perspective, substituting fossil natural gas with biogenic methane across the auxiliary burner and SMR processes yields a net-zero climate impact under standard IPCC accounting frameworks. The proposed plant configuration avoids approximately 297 $kgCO_2/h$ in direct emissions, corresponding to an annual greenhouse gas mitigation of nearly 2,400 tCO_2.

Future work will optimise key operating conditions to improve plant efficiency. Sensitivity analyses will assess how pressure and temperature affect syngas yield and PEMFC performance. A key focus is on reducing parasitic loads, especially the cathode air compressor. By studying lower-pressure operation and better thermal integration, the aim is to maximise net electrical power by balancing stack voltage gains against Balance-of-Plant (BoP) power consumption.

Acknowledgments

The authors gratefully acknowledge Ingenia S.r.l. for its collaboration with the Department of Industrial Engineering and Mathematical Sciences (DIISM), Marche Polytechnic University (UNIVPM), for providing the biomethane flow rate and composition data used in this analysis, and for fully funding the Ph.D. scholarship of Eng. Benedicta Croce, first author of this research work.

Nomenclature

A	Active area, cm^2
E	Electrical potential, V
F	Faraday constant, C/mol
I	Cell current, A
i	Current density, A/cm^2
L	Catalyst loading, mg/cm^2
n	Number of electrons exchanged, -
P	Partial pressure, Pa
Q	Thermal power, kW
R	Electrical resistance, $\Omega \cdot cm^2$
R	Universal gas constant, J/(mol K)
T	Temperature, K
U	Utilisation factor, -
V	Voltage or overpotential, V

Greek symbols

α	Charge transfer coefficient, -
δ	Membrane thickness, μm
σ	Membrane ionic conductivity, S/m

Subscripts and superscripts

0	Standard conditions
a	Anode
act	Activation
c	Cathode
cell	Fuel cell
conc	Concentration
f	Fuel
L	Limiting
Nernst	Nernst
o	Exchange
Ohm	Ohmic
Pt	Platinum
ref	Reference
tn	Thermoneutral

References

[1] Antonini C., Treyer K., Streb A., van der Spek M., Bauer C., Mazzotti M., Hydrogen production from natural gas and biomethane with carbon capture and storage - a techno-environmental analysis. Sustainable Energy Fuels 2020;4:2967-86.

[2] O'Neill K.T., Jiao F., Al Ghafri S., May E.F., Johns M.L., Stable electrolytic hydrogen production using renewable energy. Energy Convers Manage 2024;321:119070.

[3] Rosa L., Mazzotti M., Potential for hydrogen production from sustainable biomass with carbon capture and storage. Renew Sustain Energy Rev 2022;157:112123.

[4] Singh D., Sirini P., Lombardi L., Green hydrogen production from biogas or landfill gas by steam reforming or dry reforming: specific production and energy requirements. Energies 2025;18:2631.

[5] Amran U.I., Ahmad A., Othman M.R., Kinetic based simulation of methane steam reforming and water gas shift for hydrogen production using Aspen Plus. Chem Eng Trans 2017;56:1681-86.

[6] Sinurat F.K., Sitorus T.B., Bin Nur T., Susilo H., Simulation analysis of polymer electrolyte membrane fuel cell using Aspen Plus. Journal of Physics: Conference Series 2020;1566(1):012024.

[7] Barelli L., Bidini G., Gallorini F., Ottaviano A., Dynamic analysis of PEMFC-based CHP systems for domestic application. Applied Energy 2012;91:13-28.

[8] Crespi E., Guandalini G., Gößling S., Campanari S., Modelling and optimization of a flexible hydrogen fueled pressurized PEMFC power plant for grid balancing purposes. Applied Energy 2021;285:116431.

[9] Aspen Technology Inc. Aspen Physical Property System: Physical Property Methods and Models. Burlington, MA, USA: Aspen Technology Inc.; 2012. Reference Manual.

[10] Santarelli M.G., Torchio M.F., Cochis P., Parameters estimation of a PEM fuel cell polarization curve and analysis of their behavior with temperature. J Power Sources 2006;159:824-35.

[11] Falcão D.S., Pinto A.M.F.R., A review on PEM electrolyzer modelling: guidelines for beginners. J Clean Prod 2020;261:121184.

[12] Wang L., Husar A., Zhou T., Liu H., A parametric study of PEM fuel cell performances. Int J Hydro Energy 2003;28:1263-72.

[13] Simpson A.P., Lutz A.E., Exergy analysis of hydrogen production via steam reforming. Int J Hydro Energy 2007;32:4811-20.

[14] Vagia E.C., Lemonidou A.A., Thermodynamic analysis of hydrogen production via steam reforming of selected components of aqueous bio-oil fraction. Int J Hydro Energy 2007;32:212-23.

[15] Reeves A., Simulation of SMR plant for hydrogen production in Aspen HYSYS [BEng dissertation]. Bradford, UK: University of Bradford; 2021.\

[16] Zolghadri S., Kiani M.R., Kamandi R., Rahimpour M.R., Enhanced hydrogen production in steam methane reforming: comparative analysis of industrial catalysts and process optimization. J Energy Inst 2024;113:101541.

[17] EG&G Technical Services Inc., Fuel cell handbook (7th ed.). Morgantown, WV, USA: U.S. Department of Energy; 2004.

[18] IPCC, 2006 IPCC Guidelines for National Greenhouse Gas Inventories. Prepared by the National Greenhouse Gas Inventories Programme, Eggleston H.S., Buendia L., Miwa K., Ngara T., Tanabe K. (eds). Hayama, Japan: IGES; 2006.